This is the accepted manuscript made available via CHORUS. The article has been published as:

Partial glass isosymmetry transition in multiferroic hexagonal ErMnO_{3}

A. Barbour, A. Alatas, Y. Liu, C. Zhu, B. M. Leu, X. Zhang, A. Sandy, M. S. Pierce, X. Wang, S.-W. Cheong, and H. You

Phys. Rev. B **93**, 054113 — Published 18 February 2016

DOI: 10.1103/PhysRevB.93.054113

Partial Glass Isosymmetry Transition in Multiferroic Hexagonal $ErMnO_3$

A. Barbour[1], A. Alatas[2], Y. Liu[1], C. Zhu[1], B.M. Leu[2], X. Zhang[2], A. Sandy[2], M.S. Pierce,[3]

X. Wang,[4] S.-W. Cheong[4], and H. You[1*]

[1]Materials Science Division, Argonne National Laboratory, IL 60439

[2]Advanced Photon Source, Argonne National Laboratory, IL 60439

[3]Rochester Institute of Technology, Department of Physics, Rochester NY, 14623

[4]Rutgers Center for Emergent Materials and Department of Physics and Astronomy, Rutgers University, Piscataway, New Jersey 08854

Abstract

Ferroelectric transitions of a hexagonal multiferroic, $ErMnO_3$, are studied by x-ray scattering techniques. An isosymmetry transition, similar to that previously observed for $YMnO_3$, approximately 300 K below the well-known ferroic transition temperature is investigated. The partial glassy behavior of the isosymmetry transition is identified by appearance of quasi-elastic scattering lines in high-energy-resolution scans. The glassy behavior is further supported by the increased interlayer decorrelation of $(\sqrt{3}\times\sqrt{3})R30^{o}$ ordering below the isosymmetry transition. The transition behavior is considered for possible hidden sluggish modes and two-step phase transitions theoretically predicted for the stacked triangular antiferromagnets. The in-plane azimuthal (orientational) ordering behaviors were also compared to the theoretical predictions. Coherent x-ray speckle measurements show unambiguously that the domain sizes decrease anomalously near both the isosymmetry and ferroic transitions. However, domain boundary fluctuations increase monotonically with an Arrhenius form with an activation energy of 0.54(5) eV through both transitions.

The submitted manuscript has been created by UChicago Argonne, LLC, Operator of Argonne National Laboratory ("Argonne"). Argonne, a U.S. Department of Energy Office of Science laboratory, is operated under Contract No. DE-AC02-06CH11357. The U.S. Government retains for itself, and others acting on its behalf, a paid-up nonexclusive, irrevocable worldwide license in said article to reproduce, prepare derivative works, distribute copies to the public, and perform publicly and display publicly, by or on behalf of the Government.

Introduction

Multiferroics are of scientific and technological interests for coupling of magnetism and ferroelectricity.[1] Among them, layered hexagonal manganites exhibit unit-cell tripling transitions and the trimerization leads to intricate vortices and domains.[2] Magnetizations are strongly coupled at domain walls due to the improper coupling of trimerization[3] to the ferroelectric order parameters[4] and some exhibits room temperature multiferroic behavior.[5] While it is well recognized[2,4] that the trimerization is key to the multiferroic behavior, the process of the trimerization, the ferroic (para-ferro) transition is not well understood. Despite that the hex-manganites were discovered long ago,[6,7] it is still under extensive investigation how the high-temperature para phase transforms to the low-temperature trimerized phase and whether or not there should be an intermediate transition.[8,9,10,11,12,13,14] We examined single crystals of $ErMnO_3$ (and $YMnO_3$)[15] with x-ray techniques to elucidate the structural and dynamical aspects of the trimerization transitions.

At high temperatures, $ErMnO_3$ forms a simple hexagonal para phase with $P6_3/mcm$ symmetry. At T_c (1195ºC), one of three Er atoms buckles out of the plane forming an antiferroelectric $\left(\sqrt{3}\times\sqrt{3}\right)R30°$ superlattice with concomitant titling of MnO_5 bipyramids (trimerization), which lowers the symmetry to $P6_3cm$.[16] In addition, hundreds of degree below T_c, the intermediate transition has been suggested in the thermal expansion measurements of $YMnO_3$ by Nénert et. al.[10] However, the neutron powder diffraction study by Gibbs' et. al.[14] did not find a symmetry change, which is expected in a real phase transition. Instead, the study found that some structure parameters, such as the total polarization, decreases suddenly and hence termed an isosymmetry transition. Our *in situ* equilibrium measurements were started with the as-grown $ErMnO_3$ single

crystals and repeated by cycling above the ferroic transition temperatures where domain patterns are expected to evolve.[2,17,18] We find also hundreds of degree below T_c that intensities of quasi-elastic lines, in non-resonant high-energy-resolution inelastic x-ray scattering (HERIX), exhibit a transition indicating a rapid change in the dynamic nature much like a glass transition. Other characteristics further supporting the glassy behavior of the transitions are also studied using conventional x-ray techniques. In addition, the domain statics and dynamics are studied with coherent x-ray speckle scattering measurements where K_3-mode activation energy at the domain boundary is obtained. Our studies are compared to theoretical studies with the Landau expansion,[19] the proposed hidden order parameter[20] for a possible origin of the glass transition behavior and a recent Monte Carlo (MC) simulation[21] where orientational order parameters are investigated.

Experimental

$ErMnO_3$ (and $YMnO_3$) crystal specimens were grown by a flux method: 10 mol. % corresponding polycrystalline powders with 90 mol. % Bi_2O_3 powders as flux were heated to 1250°C, and then slowly cooled to 800°C in a platinum crucible. The shape of the sample was plates of 1~3 mm and ~0.1 mm in thickness. The surfaces of the samples were (0 0 1) planes without exception. The fresh samples are shiny, reflecting ambient light with few defects. In fact, the fresh surfaces exhibit well-defined atomic step structures.[15] However, the samples can lose the luster over the course of several days in air at high temperature. This was much more evident in $YMnO_3$ samples.[15] For the reason, $YMnO_3$ was not as much studied here as $ErMnO_3$.

Samples were affixed with a thin layer of high-temperature paste on a 1 cm cylindrical platinum crystal that is inductively heated to a desired temperature. The sample temperature was measured with a *K*-type thermocouple spot-welded to the platinum crystal and additionally calibrated by the platinum thermal expansion. Finally the temperature of the sample was calibrated against the platinum temperature using a pyrometer. We estimate the accuracy of absolute temperature is limited by the pyrometer readings of the sample and platinum to ±25° and the relative accuracy is limited by the thermocouple to ±5°.

X-ray integrated-intensity measurements and *H* and *L* scans were performed with in-house rotating anode x-rays. Lattice constant measurements, coherent x-ray scattering, and HERIX were performed at 11ID-D, 8ID-E and 3ID-C beamlines, respectively, at Advanced Photon Source (APS), Argonne National Laboratory. The lattice constants were measured with a wavelength of 1.07812 Å. A Pilatus 200(h)×1000(v) pixel detector with a pixel size of 0.175 mm was used as a detector. A region of interest was set to 2 pixels vertically to maintain ~0.4 mrad resolutions in the vertical 2θ scan directions while the detected intensities along the other direction are integrated. The *a*-axis lattice constant was measured with (1 1 0.15) in a glancing incidence geometry. Because the thin sample was affixed with paste to the platinum crystal surface for heating, access to an in-plane peak was possible only in glancing-incidence reflection geometry. HERIX experiments were performed using energy-variable six-bounce monochromator at the x-ray energy of 21.657 keV.[22] Fixed back-scattering analyzers were used achieving ~2 meV energy resolution.[23] Four analyzers, spaced at fixed Δ2θ angular distances, were mounted on the horizontally scanning 2θ arm for simultaneous data acquisitions. Coherent x-ray experiments were performed with a single bounce Si (111) monochromator setting the photon energy to 7.36 keV. The beam was vertically focused to 3 μm by a kinoform[24] lens with

the acceptance of ~100 μm set by a vertical slits and horizontally unfocused to the size of 10 μm set by horizontal slits. This beam profile delivers a sufficient transverse coherence for reflection coherent x-ray experiments where the path length differences from the surface layers are much less than the longitudinal coherence length. The detector was an x-ray sensitive charge coupled device with a pixel size of 25 μm and mounted on the 2θ arm at a distance of 1 m from the sample. The correlation time in our reflection experiment with a static sample was over 10^5 sec.[25,26]

Results and Discussion

The lattice expansion measured in synchrotron high-momentum-resolution measurements shows an anisotropic behavior. The measured *a* and *c* lattice parameters are shown in Figure 1 with the known room-temperature lattice constants.[3] *a* lattice constant (left abscissa) expands without any hint of the intermediate transition. In fact, there is no hint of a transition even at T_c and a straight line can fit over the entire temperature range that we measured. Yet; there are interesting features in *c* lattice constant (right abscissa): little or slow expansion up to ~350ºC, linear *contraction*, not expansion, to 880ºC, acceleration of the contraction between 880ºC and T_c, and no further contraction above T_c. This indicates that only *c* axis negative expansion is sensitive to phase transitions while *a* axis simply ignores the transitions and follows a linear thermal expansion. This anisotropic expansion behavior and the slope discontinuity[27] at 880ºC provide initial clues for understanding the transition behaviors.

The tripling order parameter, measured with the intensity of (1 0 4) reflection, shows an anomaly at 880ºC, otherwise exhibiting a power law behavior. In x-ray scattering measurements,

because scattering factor of Er is much larger than those of Mn and O, the buckled Er atoms contribute primarily to the unit-cell tripling reflections such as (1 0 L). The intensity is proportional to $|\delta \cdot L|^2$, where δ is the out-of-plane distance between Er atoms, and represents the square of the corresponding order parameter, which in turn closely resembles the antiferroelectric order parameter.[28] On close examinations of the (1 0 L) intensities, we found that the intensities of (1 0 L) does not change monotonically even though the behavior close to T_c follows a power-law. This is evident in (1 0 4) shown in Figure 2(a). We find that the (1 0 4) intensity near T_c between 900°C and 1195°C fits very well with $\propto(1195-T)^{2\beta}$ with β=0.25(1) (black solid line). However, the (1 0 4) intensity deviates significantly from the solid line below 900°C where we found the *c* lattice (Figure 1) slope discontinuity. Therefore, we drew another solid line with a similar function (blue line), $\propto(880-T)^{0.5}$. Henceforth, we denote tentatively this intermediate isosymmetry transition[14] at 880ºC as T^*.[21]

Below T^* transition, the quasi-elastic line intensity *increases* as temperature *decreases*. Selected HERIX scans at (1.05 0 4) and (0.75 0 2.95) are shown in Figure 3 (a) and (b), respectively. (1.05 0 4) is chosen to be near but not precisely at (1 0 4) and (0.75 0 2.95) is one of the three accompanying detectors[29] chosen for the odd L value (2.95≈3). In both cases, there are unusually large central quasi-elastic peaks, in both (a) and (b), albeit truncated to show the transition better. Their integrated intensities of the quasi-elastic peaks are summarized in Figure 2(b) with a solid line of $\propto(880-T)^{0.5}$. The quasi-elastic peak appears at T^* and its intensity increases as T decreases. The quasi-elastic peak intensity is expected to be zero or weak away from Γ (Bragg) points for ideal lattices. The strong quasi-elastic peak indicates that there are static, frozen, over-damped, or sluggish modes because the quasi-elastic x-ray measurements are

essentially long-exposure average of the corresponding Fourier component over ~ps or longer. We find at room temperature that the quasi-elastic intensity of (1±η 0 4) drops rapidly as η (η≪1) increases, indicating that the frozen or sluggish modes are due to imperfect $\left(\sqrt{3}\times\sqrt{3}\right)R30°$ ordering. The amplitudes of frozen or sluggish modes are large at low temperature and gradually unfreezes at T^* as T increases much like a behavior of a glass. This behavior is also similar to the behavior of $Pb(Mn_{1/3},Nb_{2/3})O_3$,[30] a prototypical relaxor. The frozen imperfections most likely suppress Γ_2^- mode, which is a primary ferroelectric mode along c-axis.[14] When the imperfections disappear, the (1 0 4) Bragg intensity jumps back up near T^* in Figure 2(a) and the $\left(\sqrt{3}\times\sqrt{3}\right)R30°$ ordering partially restores. In Figure 3(b) of the energy scans at (0.75 0 2.95), independent of the ordering for its odd L values, the quasi-elastic peaks are weak. The glassy behavior disappears above T^*. Both quasi-elastic intensities increase with $(T-T^*)^2$. This happens when the interlayer stacking order is high near T^* but gradually decreases as T increases. The increase of the quasi-elastic peak intensity, $\propto(T-T^*)^2$, indicates that the interlayer misalignment vector, $\boldsymbol{\varepsilon}$, increases with T since $I_{misfit}\propto|\boldsymbol{\varepsilon}\cdot\mathbf{Q}|^2$ for small misalignments.[30] The continued increase even above T_c indicates that short-range Er buckling still exists similarly to Y atoms.[14]

The increased stacking correlation near T^* is additionally confirmed in conventional diffraction experiments. In Figure 4(a), we show the measured full width half maximum (FWHM) of L-scans through (1 0 4) reflection vs. T by squares. We find that FWHM decreases almost to that of the instrumental resolution, ~0.01 reciprocal lattice unit (r.l.u.) as $T \rightarrow T^*$. From the width, we calculated the correlation length (circles) using the relation, $\xi = c\,2\sqrt{2\ln 2}\Big/\sqrt{\left(\sigma^2-\sigma_0^2\right)}$ where ξ, σ, and σ_0 are correlation length, FWHM, and the instrumental resolution, respectively. The fits

to the *L*-scans were made with a pseudo-Voigt function. However, the Lorentzian component was small and did not change much over the entire temperature range. It shows that the interlayer stacking correlation length diverges at T^*. The widths of in-plane radial and azimuthal scans are shown in Figure 4(b). The widths of the azimuthal scans behave similarly to those of the *L* scans albeit a bit more complex. Note that the widths of the radial scans do not change significantly over the same temperature range. (The weak *T*-dependence seen here is largely due to the resolution envelope overlapping with the azimuthal scans.) Again, we show that the interlayer correlations are low (large widths) at low temperature and increase as *T* increases to T^*, which is opposite to the property of ordinary crystalline materials and the prediction of recent MC study.[21] This is significant because the MC prediction agrees well above T^* [see Figure 4(b)] when the behavior returns to that of ordinary crystalline materials above T^*. Namely, the interlayer stacking azimuthal correlation drops (the azimuthal width increases) significantly as expected approaching T_c. Below T^*, however, we believe it does because the glassy behavior takes over the azimuthal correlation.

Considering anisotropic lattice expansion, quasi-elastic intensity, and scan widths discussed above suggest that the stacking correlation of the superstructure changes at T^* with little or no in-plane superstructure disorder. One way to elucidate the nature of the two-step transition behavior is to compare with previous phase-transition studies. Based on the behavior of the transition near T_c, we expect that the transition is of a 2^{nd} order or weakly first order. In a mean-field terminology, this value of β indicates a critical transition through the tricritical point. This is unlikely and we may consider the transition behavior beyond the mean-field approximation by mapping the Er displacement to Ising magnets on a stacked triangular lattice. Ising magnets on a stacked triangular lattice are a frustrated system and have been studied theoretically [31,32] and

experimentally.[33] In particular, a Monte Carlo (MC) S=∞ simulation study[34] is interesting as the magnetization, $|M|$, exhibits the two-step transition that is qualitative similar to T^* and T_c seen the (1 0 4) intensityFigure 2(a). The two steps are a transition from the ferrimagnetic (FR) structure to a partially disordered (PD) structure at $k_B T^* / J = 0.8$ and another from PD to para magnetization at $k_B T_c / J = 1.2$. In addition, our exponent, β=0.25, is in remarkable agreement with the theoretical study[32] that is confirmed in the neutron diffraction.[33] Another critical exponent ν=0.53 of the model[32] can also be considered as indicated by the solid red line in Figure 4, $\xi = \alpha(1 - T/880)^{-\nu}$, with the fit value of α=1.7(1)×10^2 Å. Therefore, we believe that the model of stacked triangular antiferromagnets is a good approach. It will be of theoretical interest to further explore dynamic and critical behaviors of the hexagonal antiferroelectrics by considering some differences. The $ErMnO_3$ has an A-B stacking hexagonal lattice, not A-A triangular lattice. More importantly, the antiferroectric trimerization must accompany MnO_5 bipyramids linking the interlayer positions of the Er trimerization, which leads to internal disordering. In fact, the possible three Er states proposed by Cano[20] can reinforce the relationship to the layered triangular antiferromagnets. In this regard, glassy aspect of the observed behavior can be considered from the perspective of short-range hidden or complex order parameter(s).[20] While the overall averaged structure has well-defined symmetry, unit cell, and atomic positions, we have shown that certain modes undergo a glass-like transition behavior, evident in dynamics of the system probably due to the complex nature of the trimerization. On the other hand, it could simply be like the glass transition,[32] which is often characterized by dynamic behavior without identifiable specific mode(s) or many modes are entangled to form a glassy state similar to spin-glass type disordering.[35,36] In a way, our observations suggest that the apparently well-defined

structure in classical sense may not be as well defined as we thought. The glassy state also explains the sudden decrease in the total polarization.[14]

While the above incoherent x-ray techniques are *in*sensitive to domain boundaries, coherent x-rays are sensitive to the domain boundaries and their fluctuations. It is well established that the $ErMnO_3$ form complex and topological domains and the domain sizes and shapes are sensitive to cooling rate[17] that is accessible within the time scales of x-ray photon correlation spectroscopy (XPCS). [37] We used the surface-sensitive speckle patterns on a crystal truncation rod (CTR).[38,39,40] The CTR x-ray speckles arise from interferences between structure factors of up (+) and down (−) terminations.[41,42,43] A simple derivation[15] yields the CTR structure factor for a fixed l from a mix of + and − domains as,

$$S_{CTR}(l,p,q) = \frac{f^{+}e^{i\Delta\phi}}{1-e^{-i2\pi l}} \iint_{S^{+}} e^{-i(px+qy)} dxdy$$

where f^{+} and $\Delta\phi$ are the amplitude of + domain and the phase difference between + and − domains, p and q momentum transfers of a given pixel and S^{+} represents the fragmented area[2] of the + domains. The calculated phase difference[15] is almost π near (004) and S_{CTR} is proportional to $2f^{+}/2\pi\Delta l$ times the integral. Note that the speckle pattern changes when domain boundaries meander or reshape. Therefore, the time-evolution of speckles is a result of domain boundary meandering while the speckle pattern is a result of domain sizes and distributions. A point of CTR, (0 0 4.125), was chosen for strong enough intensity for XPCS analysis and sufficient sensitivity to near surface domain structures ($\Delta l = 1/8$, 8 unit cells, or ~10 nm deep).[15]

The two-step transitions are also evident in domain dynamics measured with coherent x-ray speckles. Examples of speckle patterns are shown in Figure 5(a)-(d). The green pixels are at

half maxima and the red and yellow pixels are above. In (e), the peak intensities (circles) and full area at half maxima (FAHM) (squares) are plotted. While the integrated intensity (peak intensity times the FAHM) shows no significant change over the temperature range, FAHM increases drastically near both T^* and T_c and drops down between them. This can also be seen from the images in (b) at 820ºC and (d) at 1170ºC where speckles spread, indicating that domain sizes are smaller below both transitions. The domains are much smaller near the ferroic transition as expected. Note, however, the spread speckles, namely small domains, from the near surface region at 820ºC do not necessarily mean on average smaller domains since the interlayer correlation is high near T^*.

The temporal behavior of the domain boundary motions can be characterized by a single thermodynamic parameter τ, correlation time, using XPCS autocorrelation analysis.[37] We plot τ vs. temperature in Figure 6. The value of τ changes more than an order of magnitude from ~20000 sec at 720ºC to <2000 sec at 1270ºC. The two-time correlation maps are also shown as insets where we can clearly compare two temperatures. The diagonal high intensity indicates that the pattern self-correlates while the off-diagonal spread indicates how rapidly the pattern de-correlates in time. A lay-term interpretation of τ, therefore, is the time elapsed for a domain pattern to lose most of the resemblance to the initial pattern due to the domain boundary meandering. For a domain boundary to meander, of course, Er atom must overcome the activation potential (see the lower inset) between the up and down domains with appropriate adjustment of the MnO_3 polyhedron. This is the essentially equivalent to K_3 phonon activation energy per unit cell. In a simple thermodynamic activation processes, we have shown that τ follows a simple Arrhenius form.[40,44] This is also true here as shown in Figure 6 with the activation energy of 0.54(5) eV. This is remarkable because the domain sizes change non-

monotonically as in Figure 5(e). This apparently counter intuitive observation has in fact a quite simple interpretation. The domain boundary energy decreases at the phase transitions while the activation energy of the moving the domain boundaries remain constant over the entire temperature ranges of the two transitions. It is also remarkable to see that the activation energy agree well with the *ab initio* calculation where the energy barrier of K_3 mode between the amplitudes of 0 Å and 0.85 Å (energy minimum) is ~0.5 eV[19] when the energies are renormalized by the ratio of T_c's for $ErMnO_3$ and $YMnO_3$.

Summary

In summary, we report an observation of partial glassy behavior of the isosymmetry dynamic phase transition of $ErMnO_3$. The dynamic nature of the transition is unambiguously defined in high-energy-resolution quasi-elastic x-ray measurements supported by interlayer correlation-length measurements. The transition appears consistent with critical behavior of stacked triangular antiferromagnets above the transition (T^*). However, the low temperature behavior below the transition is much like that of glasses even though the average structure is well described by the $P6_3cm$ symmetry. We propose that the system behaves like a stacked triangular spin glasses where the random interactions are provided by MnO_5 interlinking bipyramids, probably controlled by hidden order parameters.[20] We believe that similar partial glass transitions exist likely in other multiferroics, and probably in other complex materials such as relaxor ferroelectrics,[45] where relevant phonon modes[46,47] are still under investigations. We also find that both isosymmetry and ferroic transitions have a strong influence on the domain structures in our coherent x-ray scattering studies. Our x-ray photon correlation spectroscopy analysis of the speckle patterns finds the K_3 mode activation energy of $ErMnO_3$ to be 0.54(5) eV.

Acknowledgement

The work (AB, CZ, HY) at Materials Science Division at Argonne National Laboratory was supported by the U.S. Department of Energy (DOE), Office of Basic Energy Sciences (BES), Materials Sciences and Engineering Division, and the work (AA, BL, AS, XZ) at the Advanced Photon Source (APS) and use of the APS by DOE BES Scientific User Facilities Division, under Contract No. DE-AC02-06CH11357. The work at Rutgers is funded by the DOE under Grant No. DE-FG02-07ER46382.

References

*Author to whom correspondence should be addressed to email: hyou@anl.gov

[1] S.-W. Cheong, M. Mostovoy, Nat. Mater., 6, 13 (2007).

[2] T. Choi, Y. Horibe, H.T. Yi, Y.J. Choi, W. Wu, and S.-W. Cheong, Nature Mater., 9, 253 (2010).

[3] B.B. van Aken, T.T.M. Palstra, A. Fillippetti, N.A. Spaldin, Nat. Mater. 3, 164 (2004).

[4] H. Das, A.L. Wysocki, Y. Geng, W. Wu, C.J. Fennie, Nat. Comm. 5, 2998 (2014).

[5] W. Wang, J. Zhao, W. Wang, Z. Gai, N. Balke, M. Chi, H.N. Lee, W. Tian, L. Zhu, X. Cheng, D.J. Keavney, J. Yi, T.Z. Ward, P.C. Snijders, H.M. Christen, W. Wu, J. Shen, X. Xu, Phys. Rev. Lett., 110, 237601 (2013).

[6] H.L. Yakel, W.C. Koehler, E.F. Bertaut, E.F. Forrat, Acta. Cryst. 16, 957 (1963).

[7] Ph.Coeuré, F.Guinet, J.C.Peuzin, G.Buisaon, E.F.Bertant, Proc. of Int'l Mtg on Ferroelectricity, Vol. 1, p332, Prague 1966.

[8] Th. Lonkai, D. G. Tomuta, U. Amann, J. Ihringer, R.W.A. Hendrikx, D.M. Többens, J.A. Mydosh, Phys. Rev. B 69, 134108 (2004).

[9] I.-K. Jeong, N. Hur, Th. Proffen, J. Appl. Cryst., 40, 730 (2007).

[10] G. Nénert, M. Pollet, S. Marinel, G.R. Blake, A. Meetsma, T.T. M Palstra, J. Phys.: Condens. Matter 19, 466212 (2007).

[11] J. Kim, Y.M. Koo, K.-S. Sohn, and N. Shin, Appl. Phys. Lett., 97, 092902 (2010).

[12] C.J. Fennie and K.M. Rabe, Phys. Rev. B 72 100103(R) (2005).

[13] J. Varignon, S. Petit, M.-B. Lepetit, arXiv:1203.1752.

[14] A.S. Gibbs, K.S. Knight, P. Lightfoot, Phys. Rev. B 83 094111 (2011).

[15] Supplementary Information.

[16] B.B. Van Aken, A. Meetsma, T.T.M. Palstra, Acta Crystallographica E57, i38-i40 (2001)

[17] S. C. Chae, N. Lee, Y. Horibe, M. Tanimura, S. Mori, B. Gao, S. Carr, and S.-W. Cheong, Phys. Rev. Lett. 108 (2012).

[18] S.C Chae, Y. Horibe, D. Y. Jeong, S. Rodan, N. Lee, and S.-W. Cheong, Proc. of Nat. Acad. of Sci., 107, 21366 (2010).

[19] S. Artyukhin, K.T. Delaney, N.A. Spaldin, M. Mostovoy, Nat. Mater. 13, 42 (2013).

[20] A. Cano, Phys. Rev. B 89, 214107 (2014).

[21] M. Lilienblum, T. Lottermoser, S. Manz, S.M. Selbach, A. Cano, M. Fiebig, Nat. Phys., 11, 1070 (2015).

[22] T. S. Toellner, A. Alatas and A. H. Said, J. Synchrotron Rad., 18, 605 (2011).

[23] A. Alatas, B. M. Leu, H. Yavas, T. S. Toellner, and E. E. Alp, Nucl. Instr. Meth. Phys. Res. A649, 166 (2011).

[24] A.F. Isakovic, A. Stein, J.B. Warren, S. Narayanan, M. Sprung, A.R. Sandy, K. Evans-Lutterodt, "Diamond Kinoform Hard X-ray Refractive Lenses: Design, Nanofabrication and Testing," J. Synch. Rad., 16, 8 (2009).

[25] M.S. Pierce, K.-C. Chang, D. C. Hennessy, V. Komanicky, M. Sprung, A. Sandy, and H. You, Phys. Rev. Lett. 103, 165501 (2009).

[26] M.S. Pierce, V. Komanicky, A. Barbour, D.C. Hennessy, C. Zhu, A. Sandy, H. You, Phys. Rev. B 86 085410 (2012).

[27] Slope discontinuity is related to heat capacity of a transition via Grüneisen parameters. See H. You, et. al., Phys. Rev. 38, 9213 (1988) and *ibid*, 43, 3660 (1991).

[28] C.J. Fennie and K.M. Rabe, Phys. Rev. B 72 100103 (2005).

[29] T. S. Toellner, A. Alatas and A. H. Said, J. Synchrotron Rad., 18, 605 (2011).

[30] H. You and Q.M. Zhang, Phys. Rev. Lett., 79, 3950 (1997).

[31] D. Blankschtein, M. Ma, A.N. Berker, G.S. Grest, C.M. Soukoulis, Phys. Rev. B 29, 5250 (1984).

[32] H. Kawamura, J. Phys. Soc. Jpn, 54, 3220 (1985).

[33] Y. Ajiro, T. Nakashima, Y. Unno, H. Kadowaki, M. Mekata, N. Achiwa, J. Phys. Soc. Jpn, 57 2648 (1988).

[34] O. Nagai, M. Kang, T. Horiguchi, H.T. Diep, Phys. Lett. A, 186 359 (1994)

[35] K. Binder and A.P. Young, Rev. Mod. Phys. 58, 901 (1986).

[36] L. Berthier and G. Biroli, Rev. Mod. Phys., 83, 587 (2011).

[37] D. Lumma, L.B. Lurio, S.G.J. Mochrie, and M. Sutton, *Rev. Sci. Inst.* 71, 3274 (2000).

[38] I. K. Robinson, Phys. Rev. B 33, 3830 (1986).

[39] I. A. Vartanyants, J.A. Pietney, J.L. Libbert, I.K. Robinson, Phys Rev B 55 13193 (1997)

[40] M. S. Pierce, K.-C. Chang, D. C. Hennessy, V. Komanicky, M. Sprung, A. Sandy, H. You, Phys. Rew. Lett. 103, 165501 (2009).

[41] Speckles are *insensitive* to the topological boundaries between α, β, and γ domains.

[42] I.K. Robinson, W.K. Washiewicz, R.T. Tung, Phys. Rev. Lett., 57, 2714 (1986).

[43] H. You, U. Welp, G.W. Crabtree, Y. Fang, S.K. Sinha, J.D. Axe, X. Jiang, S.C. Moss, Phys. Rev. B. 45, 5107 (1992).

[44] M. S. Pierce, D. C. Hennessy, K.-C. Chang, V. Komanicky, J. Strzalka, A. Sandy, A. Barbour, H. You, Appl. Phys. Lett. 99, 121910 (2011).

[45] V. Westphal, W. Kleemann, and M. D. Glinchuk, Phys. Rev. Lett. 68, 847 (1992)

[46] H. You and Q.M. Zhang, Phys. Rev. Lett., 79, 3950 (1997).

[47] I. P. Swainson, C. Stock, P. M. Gehring, Guangyong Xu, K. Hirota, Y. Qiu, H. Luo, X. Zhao, J.-F. Li, and D. Viehland, Phys. Rev. B 79, 224301 (2009).

Figures

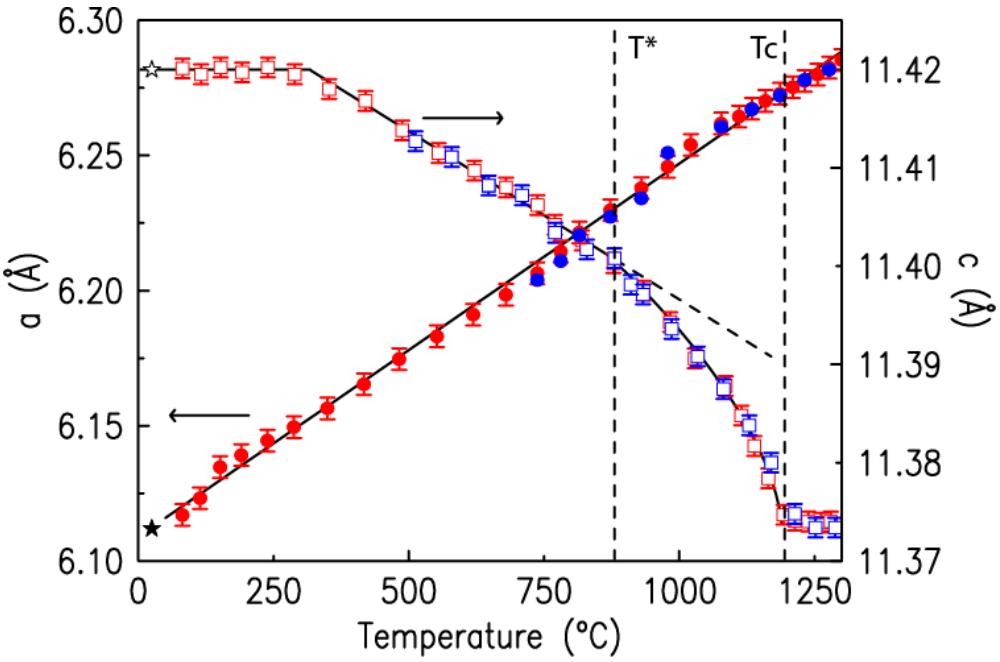

Figure 1. Lattice constants of $ErMnO_3$: *a* (filled circles) and *c* (open squares) are measured in heating (red symbols) and in cooling (blue symbols). The filled and open stars at 25ºC are from Ref. 3. The thermal expansion rate of *a* is $1.38(2)\times10^{-4}$ and that of *c* varies from 0 to -6×10^{-5}.

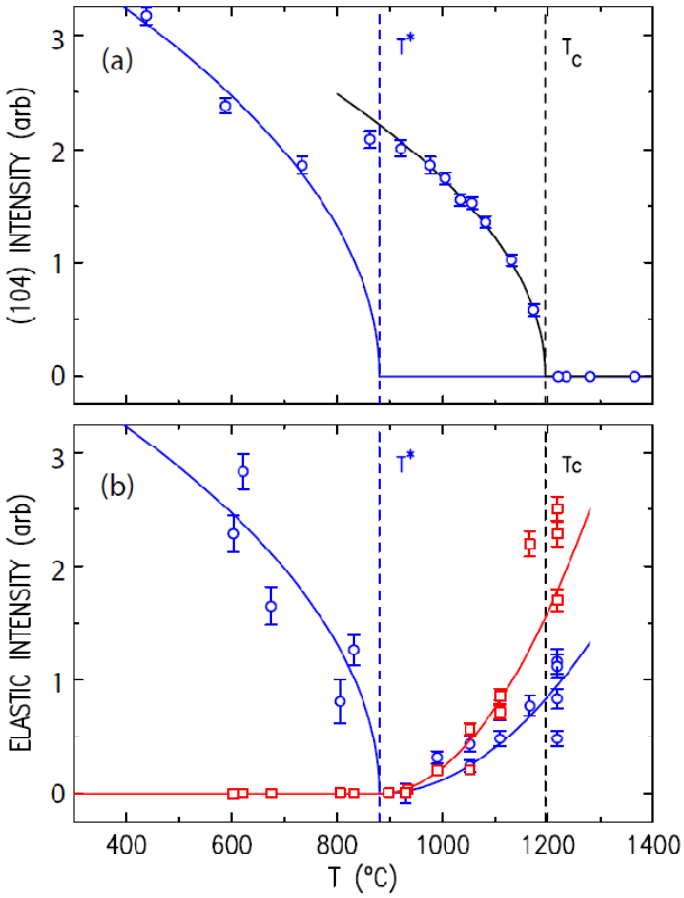

Figure 2. (a) Integrated Intensity of (1 0 4) vs. *T*. (b) Quasi-elastic Intensity vs. *T* at (1.05 0 4) (circles) and (0.75 0 2.95) (squares).

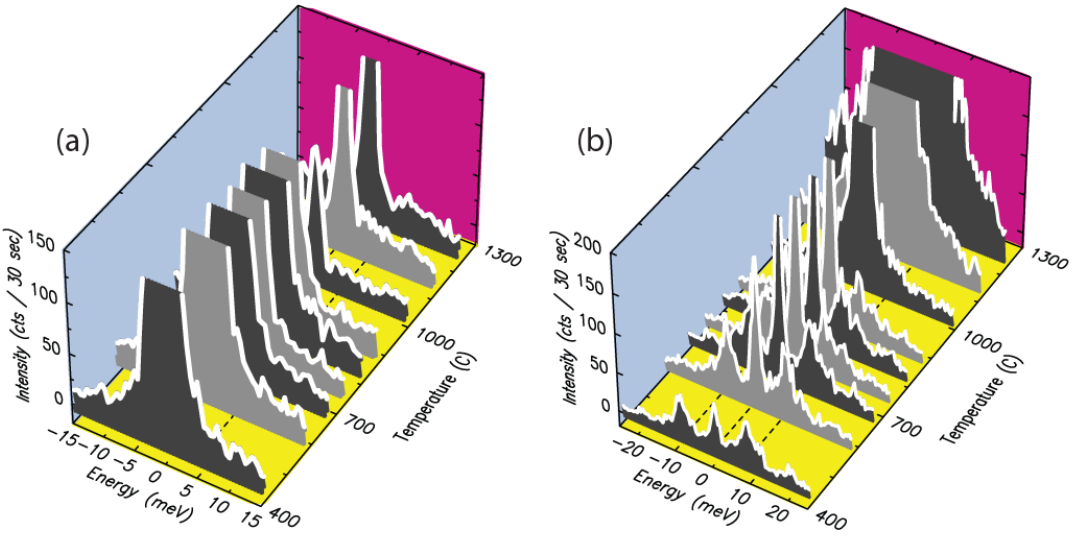

Figure 3. HERIX scans at (1.05 0 4) (a) and (0.75 0 2.95) (b). The dashed lines are 0 and ±8 meV. The intensities are truncated at 150 and 200 for clarity.

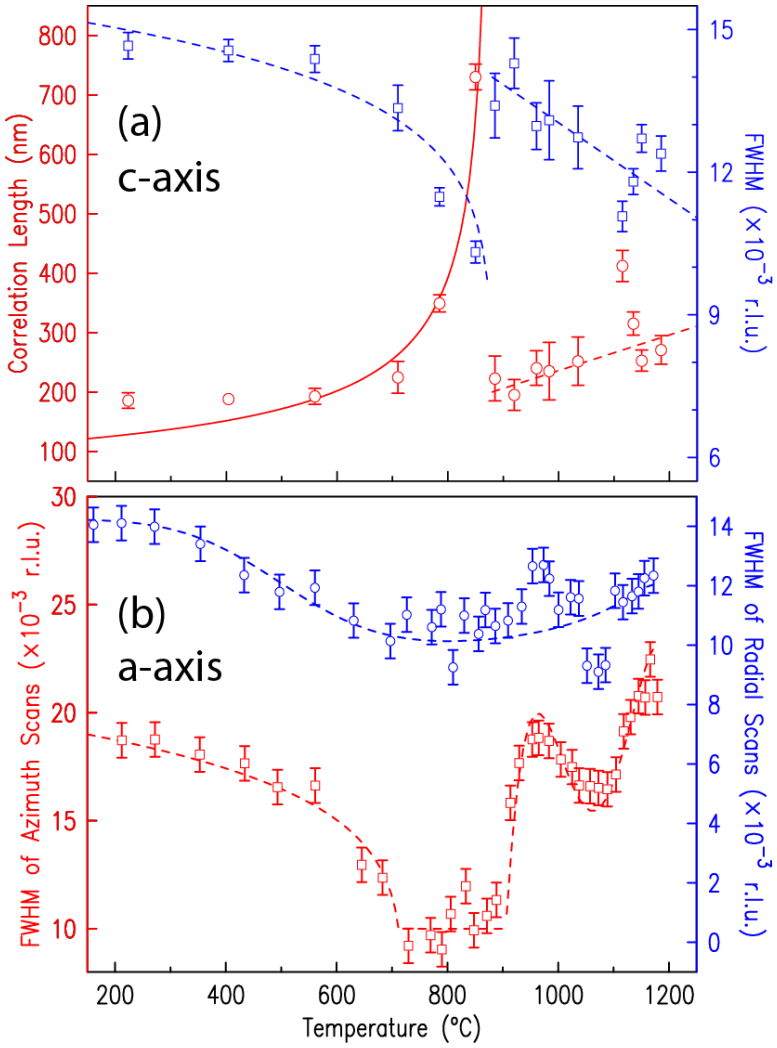

Figure 4. Scan widths of (1 0 4) along *L* (a), *H* (b, circles), and *H*-2 (b, squares) directions are plotted vs. *T*. The solid red line in (a) is a power law with the exponent ν=0.53.[32] The dashed lines are guides to the eye.

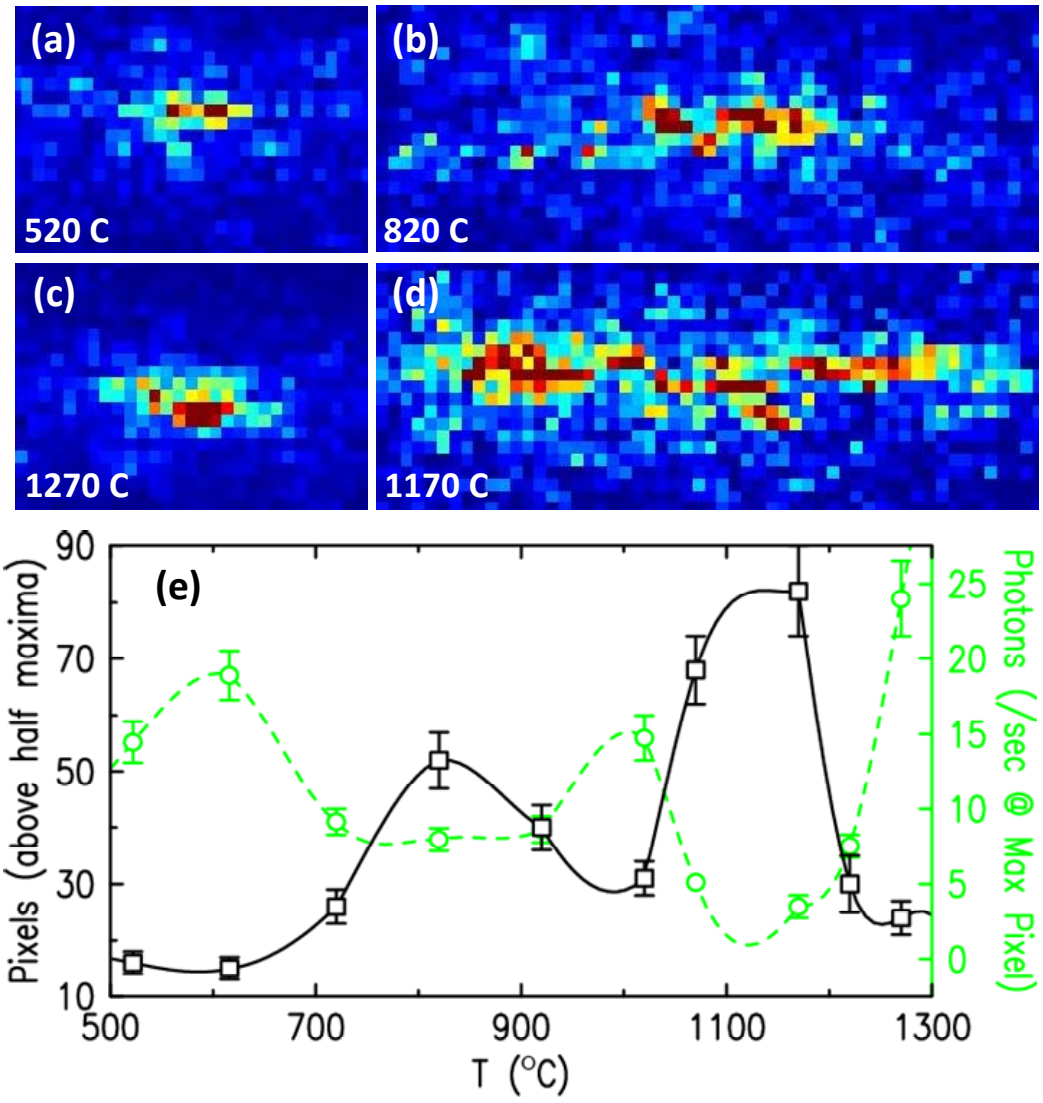

Figure 5. (a)-(d) Speckles measured at the respective temperatures. (e) Squares are numbers of the pixels above the half maxima and the circles are peak intensities per pixel averaged from 4 pixels of highest intensities. The lines are guides to eyes.

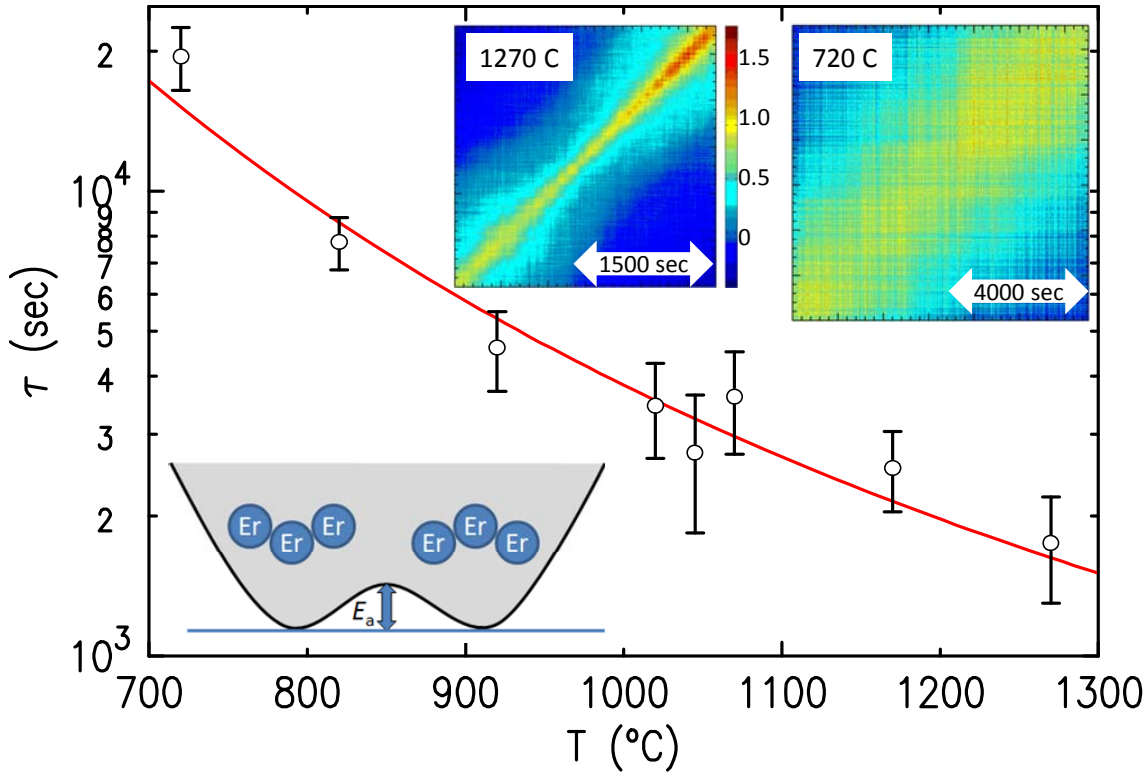

Figure 6. Correlation time of domain boundary dynamics is plotted against temperature. The solid line is the fit with the activation energy of 0.54(5) eV. The upper insets are two-time correlations for 1270 K and 720 K and the lower inset shows schematically configurations of Er positions and the activation energy.